Stacked modulation formats enabling highest-sensitivity optical free-space links

Alexandra Ludwig,[1,6] Marc-Lorenzo Schulz,[2] Philipp Schindler,[3] Stefan Wolf,[4] Christian Koos,[4] Wolfgang Freude,[4,7] and Juerg Leuthold[5,8]

[1]*Now with: Rosenberger Hochfrequenztechnik GmbH & Co. KG, 84526 Fridolfing, Germany*
[2]*Now with: Keysight Technologies, 71034 Böblingen, Germany*
[3]*Now with: Infinera Corporation, Sunnyvale, USA*
[4]*Karlsruhe Institute of Technology (KIT), Institute IPQ, 76131 Karlsruhe, Germany*
[5]*ETH Zurich, Institute of Electromagnetic Fields (IEF), 8092 Zurich, Switzerland*
[6]*Alexandra.Ludwig@rosenberger.de*
[7]*W.Freude@kit.edu*
[8]*JuergLeuthold@ethz.ch*

Abstract: A new modulation scheme with a sensitivity of 2.3 photons per bit at a bit-error ratio (BER) of 10^{-3} is discussed theoretically and demonstrated experimentally. We achieve a limiting sensitivity of 2.3 photons per bit (3.7 dB photons per bit) by stacking the modulation formats 64PPM, 4FSK and polarization-switched (PS) QPSK. This modulation stack encodes 11 bit per symbol (PPM: 6 bit, FSK: 2 bit, PS-PQSK: 3 bit). We also replaced 4FSK by 2ODFM (2-channel multiplex) for comparison. With 64PPM-2OFDM-PS-QPSK a total of 12 bit are encoded (PPM: 6 bit, 2 OFDM channels with PS-QPSK: 2 × 3 bit). Both modulation stacks show a similar limiting sensitivity and are probably the highest sensitivities so far reported for a BER of 10^{-3}. Our theoretical considerations are supported by simulations and experiments.

OCIS codes: (060.1660) Coherent communications; (060.2605) Free-space optical communication; (060.4080) Modulation.

References and links

1. D. O. Caplan, "Laser communication transmitter and receiver design," in *Free-Space Laser Communications: Principles and Advances*, J. C. R. Arun K. Majumdar, ed. (Springer, 2005), pp. 109–246.
2. M. Pfennigbauer, W. R. Leeb, M. Aspelmeyer, T. Jennewein, and A. Zeilinger, "Free-Space Optical Quantum Key Distribution Using Intersatellite Links," in *Intersatellite Link Workshop*, (Proccedings of the CNES, 2003)
3. P. J. Winzer, "Modulation and multiplexing in optical communications," in *Conference on Lasers and Electro-Optics/International Quantum Electronics Conference*, Technical Digest (CD) (Optical Society of America, 2009), paper CTuL3.
4. D. O. Caplan, "High-Performance Free-Space Laser Communications and Future Trends," in *Optical Amplifiers and Their Applications*, Technical Digest (CD) (Optical Society of America, 2005), paper TuB1.
5. D. O. Caplan, J. J. Carney, and S. Constantine, "Parallel direct modulation laser transmitters for high-speed high-sensitivity laser communications," in *CLEO:2011 - Laser Applications to Photonic Applications*, Technical Digest (CD) (Optical Society of America, 2011), Postdeadline Paper PDPB12.
6. B. S. Robinson, "Semiconductor-Based All-Optical Switching for Optical Time-Division Multiplexed Networks," (Massachusetts Institute of Technology, PhD Thesis, 2003).
7. M. Karlsson and E. Agrell, "Multilevel pulse-position modulation for optical power-efficient communication," Opt. Express **19**(26), B799–B804 (2011).
8. X. Liu, S. Chandrasekhar, T. H. Wood, R. W. Tkach, P. J. Winzer, E. C. Burrows, and A. R. Chraplyvy, "M-ary pulse-position modulation and frequency-shift keying with additional polarization/phase modulation for high-sensitivity optical transmission," Opt. Express **19**(26), B868–B881 (2011).
9. M. Karlsson and E. Agrell, "Which is the most power-efficient modulation format in optical links?" Opt. Express **17**(13), 10814–10819 (2009).
10. E. Agrell and M. Karlsson, "Power-efficient modulation formats in coherent transmission systems," J. Lightwave Technol. **27**(22), 5115–5126 (2009).
11. A. Ludwig, M.-L. Schulz, P. Schindler, R. Schmogrow, A. Mustafa, B. Moos, S. Brunsch, T. Dippon, D. Malsam, D. Hillerkuss, F. Roos, W. Freude, C. G. Koos, and J. Leuthold, "Stacking PS-QPSK and 64PPM for Long-Range Free-Space Transmission," in *Advanced Photonics 2013*, OSA Technical Digest (Optical Society of America, 2013), paper NW2C.2.

#238307 Received 17 Apr 2015; revised 21 Jun 2015; accepted 26 Jul 2015; published 13 Aug 2015

12. T. A. Eriksson, P. Johannisson, M. Sjodin, E. Agrell, P. A. Andrekson, and M. Karlsson, "Frequency and polarization switched QPSK," in *European Conference on Optical Communication (ECOC)*, Technical Digest (CD) (Optical Society of America, 2013), paper Th2D4.
13. K. Kikuchi and M. Osaki, "Highly-sensitive coherent optical detection of M-ary frequency-shift keying signal," Opt. Express **19**(26), B32–B39 (2011).
14. M. L. Stevens, D. O. Caplan, B. S. Robinson, D. M. Boroson, and A. L. Kachelmyer, "Optical homodyne PSK demonstration of 1.5 photons per bit at 156 Mbps with rate-(1/2) turbo coding," Opt. Express **16**(14), 10412–10420 (2008).
15. D. J. Geisler, T. M. Yarnall, W. E. Keicher, M. L. Stevens, A. M. Fletcher, R. R. Parenti, D. O. Caplan, and S. A. Hamilton, "Demonstration of 2.1 Photon-Per-Bit Sensitivity for BPSK at 9.94-Gb/s with Rate-1/2 FEC," in *Optical Fiber Communication Conference/National Fiber Optic Engineers Conference 2013*, OSA Technical Digest (Optical Society of America, 2013), paper OM2C.6.
16. I. T. U. Telecommunication Standardization Sector, "Forward Error Correction for High Bit Rate DWDM Submarine Systems, G. 975.1," (*www.itu.int/rec/T-REC-G.975.1-200402-I/en*, Feb. 2004).
17. R. J. Essiambre, G. Kramer, P. Winzer, G. Foschini, and B. Goebel, "Capacity Limits of Optical Fiber Networks," J. Lightwave Technol. **28**(4), 662–701 (2010).
18. W. Shieh, H. Bao, and Y. Tang, "Coherent optical OFDM: theory and design," Opt. Express **16**(2), 841–859 (2008).
19. L. C. Andrews and R. L. Phillips, *Laser Beam Propagation through Random Media* (SPIE-The international Society for Optical Engineering, 2005).
20. R. H. Barker, "Group synchonizing of binary digital systems," in *Communication Theory*, W. Jackson, ed. (1953), pp. 273–287.
21. J. G. Proakis and M. Salehi, *Digital Communications,* 5th ed. (McGraw-Hill, 2008).
22. T. Marshall, B. Szafraniec, and B. Nebendahl, "Kalman filter carrier and polarization-state tracking," Opt. Lett. **35**(13), 2203–2205 (2010).
23. K. P. Ho, *Phase-Modulated Optical Communication Systems* (Springer Science + Business Media, Inc., 2005).
24. G. Jacobsen, *Noise in Digital Optical Transmission Systems* (Artech House, Inc., 1994).
25. C. Walck, *Hand-book on Statistical Distributions for Experimentalists*, Internal Report (Universitet Stockholms, 1996).
26. M. K. Simon, S. M. Hinedi, and W. C. Lindsey, *Digital Communication Techniques, Signal Design and Detection* (Prentice-Hall, 1994).

1. Introduction

Optical free-space transmission systems for long-range applications like optical satellite communication systems need to cope with tremendous losses, because in-line amplification is not possible [1]. Therefore, any receiver has to operate reliably even with a very small number of received photons per bit. For improving the received signal power one could increase the numerical aperture of the transmitter or receiver optics, however, the achievable gain is limited by geometrical size and by pointing accuracy. So for instance, for an inter-satellite link of two geostationary (GEO) satellites a link loss of 55 dB has to be accepted [2]. Such demanding requirements call for a modulation format that offers the highest possible sensitivity.

Whenever high sensitivity is of primary interest while spectral efficiency takes a secondary rank only, pulse-position modulation (PPM) is the best choice [3]. In the past, PPM has mostly been used in direct detection receivers where the format proved to result in unbeaten sensitivity if a large number M of time slots was employed [1,4–7]. For a given data rate, however, an M-fold bandwidth is required as compared to simple on-off keying (OOK) with the same data rate. Thus, to increase the data rate over that of PPM alone, 16PPM in combination with polarization-multiplexed (PM) quadrature phase shift keying (PM-QPSK) has been used [7], and a limiting sensitivity of 3.5 photons per bit (PPB) at a bit error ratio (BER) of 10^{-3} was demonstrated [8]. This sensitivity can be further enhanced by replacing the PM-QPSK format with polarization-switched QPSK (PS-QPSK) [7], which recently intruded as the most power-efficient modulation format among the common PSK signaling types [9,10]. And indeed, stacking 64PPM and PS-QPSK results in 2.6 PPB at a BER of 10^{-3} [11].

While all these experiments show remarkable sensitivities, there is still room for improvement by exploiting another degree of freedom, namely frequency-shift keying (FSK) [12]. So far, FSK is rarely found in optical transmission. This is due to the fact that, similar to PPM, a high number of frequencies and a large receiver bandwidth is required for achieving a better sensitivity. Using FSK, a sensitivity of 3.5 PPB at a BER of 10^{-3} has recently been shown with a single-polarization using 256 frequencies and coherent detection [13].

#238307 Received 17 Apr 2015; revised 21 Jun 2015; accepted 26 Jul 2015; published 13 Aug 2015

The sensitivity of all aforementioned schemes can be further improved with the help of strong error detection and correction (FEC) [14], for instance by employing turbo coding. As an example, it has been shown that a sensitivity of 2.1 PPB is possible for BPSK with a 100% overhead that allows to correct a signal with a BER of 10^{-1} [15].

In this paper we report on improving the sensitivity to 2.3 PPB (3.7 dB) for a raw BER of 10^{-3} by stacking 64PPM with 4FSK and PS-QPSK. A pre-FEC of 4.45×10^{-3} allows the use of a standard FEC with only 7% overhead for a final BER of 10^{-15} [16]. These are to best of our knowledge the highest sensitivities so far reported for a BER of 10^{-3}.

2. Stacking modulation formats

For a transmission system where a high receiver sensitivity is to be combined with a reasonably large data rate, a modulation format must be chosen where for a given maximum average transmitter power the symbols have a large Euclidean distance while the number of encoded bits per symbol is still acceptably good.

In [9,10] Karlsson and Agrell have already shown that PS-QPSK is the modulation format with the largest possible Euclidean distance between symbols. PS-QPSK encodes 3 bits per symbol by stacking binary polarization-shift keying with QPSK [8,17].

The number of encoded bits per symbol can be increased by exploiting other degrees of freedom in the transmitted optical field strength. The previous discussion tacitly assumed that the PS-QPSK symbols occupy consecutive time intervals, the width of which determines the symbol duration (the symbol period). However, if each symbol period is subdivided in M time slots, and the PS-QPSK symbol is assigned to 1 out of these M possible time slots, we form a modulation stack of pulse position modulation (PPM) and PS-QPSK. The information content of this new symbol increases by $\log_2 M$. Assuming the same symbol duration and the same average power as before, the peak power in the occupied time slot and the required bandwidth increase by M. The high peak power together with the increased information content per symbol allows to reduce the required number of photons per bit at the receiver and thus to increase the sensitivity. The spectral efficiency is decreased though. Yet, if it is sensitivity that is most important, this could be worth the price [11]. In addition, the modulation stack can be extended by *N*-ary FSK. This increases the information content of the symbol by another factor $\log_2 N$ and reduces the required number of photons per bit even more – at the price of another reduction of spectral efficiency.

In the quest for the ultimate sensitivity one should also weigh in the options provided by multiplexing techniques. Multiplexing typically comes at the price of increased transmitter power. As an example: In the transition from PS-QPSK to polarization multiplexed (PM) QPSK one wins 1 bit of information per symbol at the price of doubling the average signal power [9,10]. Another option for multiplexing is applying wavelength division multiplexing (WDM) [3] or orthogonal frequency division multiplexing (OFDM) [18]. While an increase of the OFDM subcarrier number *N* increases the spectral efficiency, the SNR per bit remains the same: Compared to one channel, two channels need double the power and transmit double the number of bits. However, channel crosstalk, quantization errors and nonlinearities might further decrease the overall sensitivity of the system. Since our goal is to reach an ultimately low number of received photons per bit, multiplexing as such is not the proper strategy. However, if multiplexing is part of a stacked modulation format, then stacking PM-QPSK and PPM might be a good compromise between increasing the number of bits per symbol and optimizing the Euclidean distance [8].

In view of the prior art as discussed in this section, we conclude that stacking the proper modulation formats reduces the required number of received photons per bit considerably. In this respect a PPM-FSK-PS-QPSK format appears to be the optimum modulation stack regarding modulation complexity and sensitivity. However, a combined modulation/multiplexing stack like PPM-OFDM-PS-QPSK with more bits per symbol but a larger limiting number of received photons per bit seems to be an interesting candidate as well. In the following we verify this statement by showing results of an implementation of a

#238307 Received 17 Apr 2015; revised 21 Jun 2015; accepted 26 Jul 2015; published 13 Aug 2015

64PPM-4FSK-PS-QPSK modulation stack with a sensitivity of 2.3 PPB compared to a 64PPM-2OFDM-PS-QPSK modulation/multiplexing stack with 2.4 PPB.

3. Operation principle and measurement setup

In this section, we explain the experimental setup. We further describe waveform generation and signal demodulation as used in the experiments and for the simulations.

3.1. Measurement setup

The measurement setup is depicted in Fig. 1. At the transmitter a fiber laser with a linewidth < 1 kHz provides 13 dBm output power at a wavelength of 1549.5 nm (f_c = 193.5 THz). Half of the power is split off and serves as a local oscillator (LO) for coherent reception. A dual-polarization (DP) IQ-modulator encodes the information on the optical carrier. An arbitrary waveform generator (AWG) is programmed to provide four synchronized offline-generated data streams. Each AWG output operates at 12 GSa/s with a voltage-swing of 0.7 V_{pp} and a 3 dB bandwidth of about 3 GHz.

The free-space channel is emulated by a variable optical attenuator (VOA). In our simplified channel model, distortions such as scintillations and turbulences are neglected, and thus our channel represents an inter-satellite link in space, where only path losses due to the divergent beam play a significant role [19]. In [2] the typical loss for an inter-satellite link between two geostationary satellites is calculated. The authors show that the link loss for bridging a distance of 45.000 km amounts to 55 dB when using two antennas with an aperture of 30 cm (using 850 nm wavelength). Yet, to overcome larger distances such as envisioned in the Mars exploration projects, much larger link loss budgets are involved. With our modulation stack we could provide a link budget of 100 dB. This would be obtained when transmitting a signal with an average power of 26 dBm, and by receiving with a sensitivity of –74 dBm. Under these conditions, our limiting sensitivity of 2.3 received photons per bit would allow to detect a 128 Mbit/s data stream.

Our receiver consists of two cascaded erbium-doped fiber amplifiers (EDFAs) with a 0.6 nm wide optical band-pass filter in-between. The first EDFA has a noise figure of 3.1 dB at 1549 nm and provides 35 dB gain. The second EDFA provides a constant output power. A manually operated polarization controller adjusts the signal such that the field strengths per symbol in both orthogonal *x* and *y*-directions (as defined by the receiver) are equal. The signal is fed into a polarization diverse coherent receiver (Pol.-Diverse Coh. Rx) consisting of a dual-polarization 90° hybrid and four balanced detectors. Two synchronized real-time oscilloscopes with sampling rates of 80 GSa/s and analog bandwidths of 32 GHz record the signals for offline processing.

The average number of photons per bit at the receiver is deduced from a calibrated power meter (PM) connected to a 50% tap coupler right in front of the receiver.

Alternatively, the optical signal-to-noise power ratio (OSNR) is measured using a high-resolution optical spectrum analyzer (OSA) that is connected to a 10% tap coupler after the first optical pre-amplifier. Average power and OSNR measurement lead to comparable results for the received number of photons per bit as will be discussed in Appendix A.

#238307 Received 17 Apr 2015; revised 21 Jun 2015; accepted 26 Jul 2015; published 13 Aug 2015

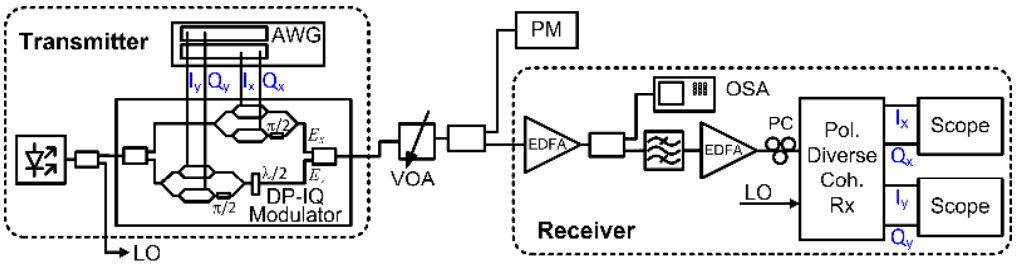

Fig. 1 Setup with transmitter and pre-amplified coherent receiver. The signal is modulated by a dual-polarization (DP) IQ-modulator driven by an arbitrary waveform generator (AWG). The free-space optical channel is emulated by a variable optical attenuator (VOA), followed by a coupler that taps the optical input and monitors the power entering the pre-amplified receiver with a power meter (PM). An optical spectrum analyzer (OSA) is used to monitor the OSNR and the polarization controlled (PC) signal is detected by a coherent polarization-diversity receiver. Two real-time oscilloscopes store the signals for offline processing. The laser acts both as a continuous-wave source for the transmitter and as a local oscillator (LO) for the receiver.

3.2. Signal generation

The waveforms with the 64PPM-4FSK-PS-QPSK symbols are generated using a Matlab program. The computed waveforms are stored in the AWG memory. The data are organized in a very long frame consisting of 2047 symbols. Each symbol comprises 64PPM slots with a slot width T_{slot} = 1.33 ns (slot rate $R_{\text{slot}} = 1 / T_{\text{slot}}$ = 750 MHz). Each PPM symbol is sampled 64×16 times. A preamble is added for PPM frame synchronization. This preamble occupies one PPM symbol and consists of a single BPSK-modulated Barker13 sequence [20]. The stored data frame is then repeated periodically to yield an uninterrupted data stream.

The 64PPM-4FSK-PS-QPSK format encodes 11 bits in one symbol. The 11 bits/symbol are derived from 11 independent pseudo-random bit sequences (PRBS), six of which are encoded in the PPM, two are encoded as FSK, and three are assigned to encode PS-QPSK.

First, the 64PPM symbols are generated. Gray coding maps 6 bit to one PPM symbol. In Fig. 2(a) the PPM symbols are displayed in the time-domain (top row), in a complex IQ constellation plane (middle row), and in the frequency domain (bottom row). A PPM symbol comprises of one pulse and many empty PPM slots.

Figure 2(b) depicts 4FSK with an orthogonal frequency spacing corresponding to the PPM slot rate R_{slot} = 750 MHz $f_{\pm1} - f_c = \pm R_{\text{slot}}$, $f_{\pm2} - f_c = \pm2\times R_{\text{slot}}$. These four tones are created by single-sideband modulation (SSB) [21]. Figure 2(b) also shows the associated frequency spectrum in the bottom row. In the phasor representation (middle row), positive (negative) frequency offsets $f_{1,2}$ ($f_{-1,-2}$) are represented by a phasor, which rotates in the mathematically positive (negative) sense.

The PS-QPSK symbols are generated by encoding 3 bits onto the 4 input signal streams $I_{x,y}$ and $Q_{x,y}$ of a dual-polarization IQ-modulator by adding an even-parity bit, i. e., the fourth bit is assigned a "0" if the sum of the three bits is even, and it is assigned a "1" if the sum is odd [10]. As a result we obtain 8 symbols as a subset of 16 possible optical states of a regular PM-QPSK. The 8 symbols of the subset are linearly polarized at an angle of $\pm45^\circ$ with respect to the *x*-polarization as defined by the receiver, and are chosen for a maximum Euclidean distance. Although the information content has decreased by one bit when going from PM-QPSK to PS-QPSK, the required number of received photons per bit has decreased, since the increase of the Euclidean distance over-compensates the loss of information content. The PS-QPSK symbols are depicted in Fig. 2(c) in the complex plane for *x*- and *y*-polarization, respectively. The two QPSK constellation diagrams depicted in Fig. 2(c) look like PM-QPSK constellations. However, the polarization switching becomes obvious, if a polarization beam splitter is inserted into the signal path with its polarization eigenstates rotated by 45° with respect to the *x*-polarization. At the bottom of Fig. 2(c) a typical NRZ spectrum for PS-QPSK is shown.

#238307 Received 17 Apr 2015; revised 21 Jun 2015; accepted 26 Jul 2015; published 13 Aug 2015

In the following, the generation of the stack is described in more detail: First, four FSK tones at $f_{\pm1} - f_c = \pm 750\,\text{MHz}$ and $f_{\pm2} - f_c = \pm 2 \times 750\,\text{MHz}$ are generated by single-sideband modulation [21]. Each tone is separated from its neighbor by an integer multiple of the PPM slot rate $R_{\text{slot}} = 1 / T_{\text{slot}} = 750$ MHz = (12 / 16) GHz, see Fig. 2(b), which corresponds to the OFDM orthogonality condition between slot duration T_{slot} and subcarrier frequency spacing. The choice of R_{slot} results from an AWG sampling rate of 12 GSa/s and 16-fold oversampling per PPM slot. We encode 2 bit on each FSK symbol and transmit one out of four possible orthogonal frequencies. The PS-QPSK symbols are encoded by appropriately modulating the phase of the $I_{x,y}$ and $Q_{x,y}$ signals which define the FSK symbol.

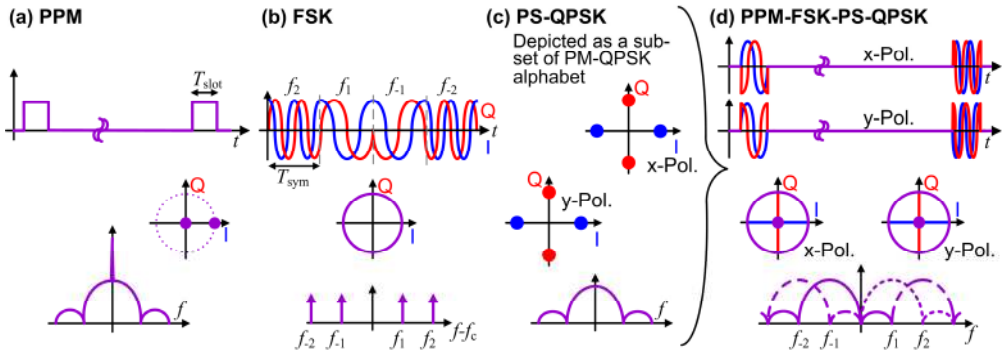

Fig. 2 Schematic display of stacking PPM with FSK and PS-QPSK symbols represented in time domain (top row), in constellation space (middle row), and in frequency domain (bottom row). The columns show typical (a) PPM, (b) FSK and (c) PS-QPSK symbols. The PS-QPSK symbols are depicted as a subset of the PM-QPSK symbols. The right-most column (d) displays the PPM-FSK-PS-QPSK stack. Each PPM pulse comprises optical sine and cosine-shaped optical fields that contain the information on the frequencies, phases and polarization.

The FSK-PS-QPSK symbols to be generated are interpreted as spectral Fourier coefficients. For 4FSK-PS-QPSK, there is one non-zero complex input coefficient per symbol and per polarization. To find the associated time-discrete $I_{x,y}$ and $Q_{x,y}$ drive signals in Fig. 1, we perform a 16-point inverse fast Fourier transform (IFFT) per symbol and per polarization. The real parts of each IFFT output represent the time-discrete version of the cosine-shaped $I_{x,y}$ drive signals, and the imaginary parts define the sine-shaped $Q_{x,y}$ drive signals. The FSK-PS-QPSK information is encoded as a phasor that rotates with a certain speed and direction with respect to a given starting point.

Besides the advantage that only one laser is required for 4FSK, our technique provides orthogonal signals as in the case of OFDM as we had mentioned before. This similarity can be exploited by transmitting more than one FSK frequency in the same PPM time slot. With two simultaneously transmitted frequencies, we combine modulation stacking and multiplexing. The limiting sensitivity achieved with this 2OFDM-PS-QPSK modulation/multiplexing stack will be later on compared with the results for a 4FSK-PS-QPSK modulation stack.

Finally, the 4FSK-PS-QPSK signals have to fill the proper non-zero PPM slots of Fig. 2(a) for completing the 64PPM-4FSK-PS-QPSK stack, see Fig. 2(d). The many empty PPM slots dominate the time-domain representation of the symbol. Each PPM pulse contains a frequency and a phase/polarization information. As shown in Fig. 2, the PPM pulse is described by the sine and cosine-shaped temporal signals with different frequencies and phases. The completed procedure explained above generates 4 time-discrete signals I_x, Q_x, I_y and Q_y that are stored in the AWG for driving the DP-QPSK modulator.

If 64PPM-2OFDM-PS-QPSK is generated, a similar procedure is applied. We use f_1 and f_2 as orthogonal subcarrier frequencies, which both are modulated with independent PS-QPSK information. We now have two non-zero complex coefficients per OFDM-PS-QPSK symbol and per polarization. As with FSK-PS-QPSK, we apply a 16-point IFFT for each PPM time slot and each polarization for generating the non-zero $I_{x,y}$ and $Q_{x,y}$ drive signals for the proper PPM time slot.

#238307 Received 17 Apr 2015; revised 21 Jun 2015; accepted 26 Jul 2015; published 13 Aug 2015

3.3. Signal demodulation

The demodulation of the received 64PPM-4FSK-PS-QPSK signal is discussed next, followed by the corresponding process for 64PPM-2OFDM-PS-QPSK.

The first steps in the demodulation process are resampling of the signal to generate a waveform with 128 samples per slot, and synchronization of the data by using the Barker13 preamble to detect the starting point of each frame. Resampling and synchronization has to be done for both polarizations, which are available at the outputs of the dual polarization 90° hybrid in Fig. 1. Each polarization carries the same PPM and FSK information.

After synchronization, we compute a 128-point fast Fourier transform (FFT) for each slot and each polarization, and evaluate the moduli of the complex output coefficients. Because the demodulation differs in part for 64PPM-4FSK-PS-QPSK and 64PPM-2OFDM-PS-QPSK formats, we describe both cases separately.

64PPM-4FSK-PS-QPSK: To extract the PPM and FSK information, the moduli of the complex output coefficients for x and y-polarization are added for each of the 64 slots. Since the 4 frequencies of the FSK tones are known, we only look for the presence of any of the 4 frequencies. The position of the maximum element within the resulting 4×64 matrix determines the location of the PPM pulse with the associated FSK information.

Next, the PS-QPSK information has to be extracted from the complex output coefficient from the FFT associated with the proper PPM slot and FSK frequency. For this, the symbols are demodulated using maximum likelihood estimation. Prior to a successful PS-QPSK demodulation we need a precise polarization alignment and phase estimation. For this a nonlinear Kalman-filter estimation algorithm [22] has been implemented. This is necessary since the manually adjusted polarization controller in front of the coherent frontend is not stable enough. For mapping the PS-QPSK data to the correct quadrant of the constellation diagrams in Fig. 2(c), the Kalman filter algorithm is modified to operate with a training sequence. To do so, an additional training sequence has been added after the synchronization preamble. This sequence consists of 25 PPM-FSK-PS-QPSK symbols with known pulse positions, frequencies, phases and polarizations. The Kalman-filter algorithm then optimizes phase and polarization alignment for each FSK frequency separately.

For a successful demodulation one should also make sure that the I and Q arms of the nested MZM in Fig. 1 are out of phase by 90°. Any phase deviation (quadrature error) leads to an elliptical IQ-plot in Fig. 2. Such a quadrature error can be corrected fairly easily in the receiver by numerically correcting phase shifts on I or Q such that the SSB signal is restored and does not have a spurious frequency component at the opposite frequency.

The received and decoded data (not including the training sequence) are compared with the transmitted data for counting the errors of the PPM, FSK and PS-QPSK reception.

64PPM-2OFDM-PS-QPSK: For this case the demodulation process is very similar to the case described above. However, the FSK demodulation step is omitted since the two OFDM carriers f_1 and f_2 in Fig. 2 are always switched on. For PPM-OFDM demodulation, the 4×64 matrix for the PPM-FSK demodulation now reduces to a vector of length 64, which contains in each of its elements the sum of the moduli of the two complex FFT values at the OFDM carrier frequencies in two polarizations, i. e., the sum of four moduli. The PPM symbol is detected by finding the maximum value in this vector. The demodulation procedure of the PS-QPSK symbols remains the same as described above. The received payload data are compared with the transmitted data for counting the errors of the PPM sequence and the two multiplexed PS-QPSK signals.

4. Theoretical sensitivity analysis of stacked modulation formats

Before reporting on the experiments we derive theoretical expressions for the sensitivity of the stacked modulation formats PPM-FSK-PS-QPSK and PPM-OFDM-PS-QPSK. Details on the theoretical receiver sensitivities for the individual modulation formats PPM, FSK and PS-QPSK are given in Appendix B.

#238307 Received 17 Apr 2015; revised 21 Jun 2015; accepted 26 Jul 2015; published 13 Aug 2015

For stacking PPM, FSK and PS-QPSK we apply and extend the approach in Ref [8]. For PPM-FSK-PS-QPSK we distinguish three cases:

1. The *M*-ary PPM symbol was detected wrongly with a symbol error probability $\mathrm{SER}_{\mathrm{PPM}}$ and an associated bit error probability $\mathrm{BER}_{\mathrm{PPM}} = \mathrm{SER}_{\mathrm{PPM}}\, M/\left(2\left(M-1\right)\right)$ according to Eq. (16) in Appendix B. In this case the detected *N*-ary FSK and PS-QPSK information is random so that on average half of their bits are wrong, i. e., the average number of erroneous bits is $\frac{1}{2}\log_2\left(N\right)$ and $\frac{1}{2}\times 3$, respectively.
2. The PPM symbol was correctly detected with a probability equal to $1-\mathrm{SER}_{\mathrm{PPM}}$, but the *N*-ary FSK symbol was detected wrongly with a symbol error probability $\mathrm{SER}_{\mathrm{FSK}}$ and an associated bit error probability $\mathrm{BER}_{\mathrm{FSK}} = \mathrm{SER}_{\mathrm{FSK}}\, N/\left(2\left(N-1\right)\right)$ according to Eq. (16) with (8) and (9), see Appendix B. In this case the detected PS-QPSK bits are random so on average half of them are wrong leading to an average number of $\frac{1}{2}\times 3$ erroneous bits.
3. The PPM and the FSK symbols were correctly detected with a probability $\left(1-\mathrm{SER}_{\mathrm{PPM}}\right)\left(1-\mathrm{SER}_{\mathrm{FSK}}\right)$, but the PS-QPSK symbol (PSQ for short) was detected wrongly with a bit error probability $\mathrm{BER}_{\mathrm{PSQ}}$ according to Eq. (21).

Because not all these cases contribute the same amount of erroneous bits, the respective bit error probabilities have to be calculated by relating the number of erroneous bits to the total number $\log_2\left(M\right)\big|_{\mathrm{PPM}} + \log_2\left(N\right)\big|_{\mathrm{FSK}} + 3\big|_{\mathrm{PS\text{-}QPSK}}$ of bits which are transmitted by the stacked *M*-PPM-*N*-FSK-PS-QPSK modulation format. As a result we find

$$\begin{aligned}\mathrm{BER}_{\mathrm{total}}^{(\mathrm{FSK})} = {} & \frac{\mathrm{SER}_{\mathrm{PPM}}\left(\frac{M}{2\left(M-1\right)}\log_2\left(M\right)+\frac{1}{2}\log_2\left(N\right)+\frac{1}{2}\times 3\right)}{\log_2\left(M\right)+\log_2\left(N\right)+3} \\ & +\left(1-\mathrm{SER}_{\mathrm{PPM}}\right)\frac{\mathrm{SER}_{\mathrm{FSK}}\left(\frac{N}{2\left(N-1\right)}\log_2\left(N\right)+\frac{1}{2}\times 3\right)}{\log_2\left(M\right)+\log_2\left(N\right)+3} \\ & +\left(1-\mathrm{SER}_{\mathrm{PPM}}\right)\left(1-\mathrm{SER}_{\mathrm{FSK}}\right)\frac{\mathrm{BER}_{\mathrm{PSQ}}\times 3}{\log_2\left(M\right)+\log_2\left(N\right)+3}.\end{aligned} \tag{1}$$

If less than 3 modulation formats are stacked, the number of transmitted bits has to be adjusted properly: Without PPM, we have $\mathrm{SER}_{\mathrm{PPM}} = 0$ and $M = 0$, without FSK $\mathrm{SER}_{\mathrm{FSK}} = 0$ and $N = 0$ hold, and without PS-QPSK we substitute 3 bit by 0 bit, i. e., we replace all occurrences of the number 3 in Eq. (1) by zero.

For 64PPM-2OFDM-PS-QPSK, the FSK-related terms in Eq. (1) do not exist, but a PS-QPSK signal is transmitted in both OFDM channels. This doubles the number of PS-QPSK bits and results in a total BER of

$$\begin{aligned}\mathrm{BER}_{\mathrm{total}}^{(\mathrm{OFDM})} = {} & \frac{\mathrm{SER}_{\mathrm{PPM}}\left(\frac{M}{2\left(M-1\right)}\cdot\log_2\left(M\right)+\frac{1}{2}\times 2\times 3\right)}{\log_2\left(M\right)+2\times 3} \\ & +\left(1-\mathrm{SER}_{\mathrm{PPM}}\right)\frac{\mathrm{BER}_{\mathrm{PSQ}}\times 2\times 3}{\log_2\left(M\right)+2\times 3}\end{aligned} \tag{2}$$

Figure 3 depicts the total calculated BER for the various stacked modulation/multiplexing formats. Figure 3(a) shows the BER versus the number of photons per bit, while Fig. 3(b) displays the BER as a function of the number of photons per symbol.

#238307 Received 17 Apr 2015; revised 21 Jun 2015; accepted 26 Jul 2015; published 13 Aug 2015

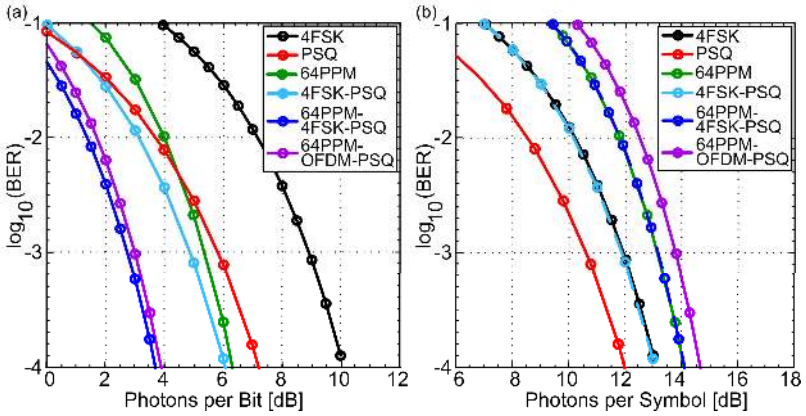

Fig. 3 Calculated bit error ratios (BER) for different modulation/multiplexing stacks. (a) BER as a function of the number of photons *per bit* (b) BER as a function of the number of photons *per symbol.*

In Fig. 3(a) it can be seen that the stacked modulation formats 64PPM-4FSK-PSQPSK and 64PPM-OFDM-PSQPSK behave similarly and require as little as 1.9 photons per bit (i.e. 2.7 dB per bit). The high sensitivity can be understood by the fact that as many as 11 and 12 bit have been encoded in one symbol of the stacked modulation formats. It is now instructive to plot the BER from Eqs. (1) and (2) as a function of photons *per symbol*, see Fig. 3(b). This plot shows that the error probability for a PS-QPSK symbol is lower than the error probability for a 4FSK format, and that the 4FSK error probability is lower than the probability for an error in the 64PPM format. The error probability for a stacked modulation format then cannot be lower than the probability of its worst constituent. Thus, the error probability per symbol for a 64PPM-4FSK-PSQPSK stack is indeed identical to the error probability of the 64PPM format, i. e., the reception is limited by the error probability of the 64PPM format. Once the PPM coding has been correctly detected, the FSK and PSQ signals are usually correctly detected as well. This becomes evident from the fact that PS-QPSK requires fewer photons per symbol. Thus, one can transmit almost two PS-QPSK symbols with the same number of photons that are required for detecting a PPM symbol. This is exactly what is done when transmitting 64PPM-2OFDM-PSQ. With 2OFDM we simultaneously transmit 2 FSK subcarriers with a PS-QPSK symbol on each subcarrier. This way we encode 6 bit in 2 OFDM carriers rather than 5 bit with the FSK-PS-QPSK stack. Because 2OFDM requires only half the optical bandwidth compared to 4FSK, the OFDM scheme is to be favored whenever the spectral efficiency in optical free-space transmission systems becomes important.

5. Experiment and simulation

To verify the theoretical prediction that PPM-FSK-PS-QPSK is among the most sensitive modulation formats, we perform simulations and experiments with the setup described in Fig. 1. For a realistic performance prediction by simulation, we match all important parameters to the experiment, namely laser power and linewidth, sampling rate and RF power of the AWG, π-voltage of the modulator, and the gain and noise figure of the EDFAs. However, the low-pass characteristics of the electrical devices at transmitter and receiver were neglected. For the simulations we used the RSoft OptSim program package.

A measurement of the received 64PPM-4FSK-PS-QPSK signal is depicted in Fig. 3. For clarity, a receiver input power of –46.5 dBm was chosen (>1000 PPB), much more than what actually would be needed for a reliable reception at $\mathrm{BER} = 10^{-3}$. In Fig. 4(a) we show four PPM symbols with duration T_{sym}. One PPM pulse per symbol can be seen. A close-up of the

#238307 Received 17 Apr 2015; revised 21 Jun 2015; accepted 26 Jul 2015; published 13 Aug 2015

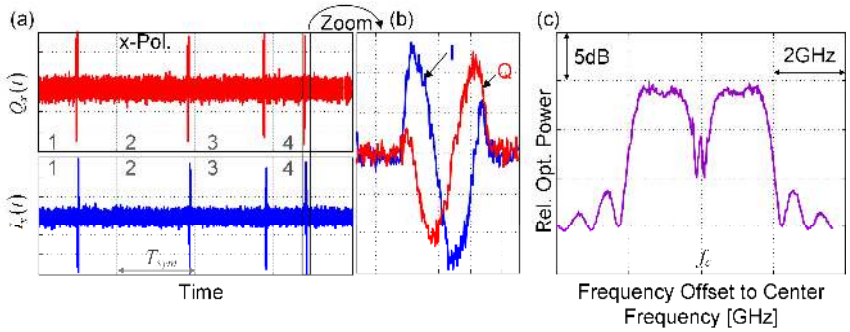

Fig. 4 Measured 64PPM-4FSK-PS-QPSK receiver signal. (a) In-phase (blue) and quadrature (red) components of a baseband signal as a function of time. The plots show the x-polarization components of 4 random symbols with symbol duration T_{sym}. (b) Zoom into the non-zero slot of the 4th symbol. (c) Optical spectrum. Four peaks at ±750 MHz and ±1.5 GHz are to be seen. The carrier f_c in the center of the spectrum is (not perfectly) suppressed.

fourth PPM symbol is shown in Fig. 4(b). Each pulse consists of sine and cosine oscillations for *I* and *Q,* respectively. Since we see only one oscillation period in Fig. 3(b), it must be frequency f_{-1} or f_1, see Fig. 2(b). Frequencies f_{-2} or f_2 would show two oscillation periods within one PPM time slot. From the phase relation between *I* and *Q* we conclude that the associated phasor rotates clockwise with angular frequency $2\pi f_{-1}$. The phases of *I* and *Q* together describe the QPSK information of the symbol. The information in the IQ components has to be retrieved by the subsequent phase-estimation algorithm.

In Fig. 4(c) the spectrum of the optical signal has been depicted. Four peaks at ± 750 MHz and ± 1.5 GHz indicate the frequencies of the FSK symbols with their modulation sidebands. The carrier frequency f_c in the center of the spectrum is only partially suppressed, due to a finite extinction ratio of the Mach-Zehnder interferometer and due to an imperfect modulator bias.

The results of sensitivity measurements together with simulations and theoretical calculations are shown in Fig. 5. The curves display the bit error ratio (BER) as a function of the number of photons per bit for our measurements (dashed lines with diamonds,—♦—), for simulations (dotted lines with + -markers,⋯ + ⋯), and for theoretical calculations (solid lines with circular markers, —○—), respectively. Kinks in the measurement curves are caused by drifting bias points of the optical modulator and due to statistical uncertainty at low BERs.

First, in Fig. 5(a), the BER for 4FSK (black) and PS-QPSK (PSQ, red) are plotted along with the BER for 64PPM (green). We then stacked two modulation formats and characterized the BER for 4FSK-PS-QPSK (light blue), see Fig. 5(b). Finally, 64PPM is added for a 64PPM-4FSK-PS-QPSK stack (blue). In this plot we also show 64PPM-2OFDM-PS-QPSK (purple). The latter modulation/multiplexing stack transports the largest information content with 12 bit/symbol, i. e., 6 bit by 64PPM and 3 bit via each of the 2 OFDM subcarriers.

For 4FSK we measure a minimum number of 9 dB photons per bit at a BER of 10^{-3} which is very close to what one would expect for orthogonal 4FSK [8]. Theoretical results given in [8] for orthogonal 4FSK are outperformed by 0.1 dB, since we aligned the polarization of the signal in the detector for reception of an equal power per symbol in the *x* and *y*- polarization, see Appendix B.

For PS-QPSK (PSQ) we find values that are reasonably close to what one would expect from theory [9,10]. PS-QPSK is predicted to have a minimum number of 5.9 dB photons per bit at a BER of 10^{-3}. In the present experiments we found a minimum number of 6.8 dB photons per bit, which is only 0.9 dB off from the theoretical limit. This offset can be explained by the non-ideal preamplifier and a non-perfect matched Rx filter used for demodulation.

#238307 Received 17 Apr 2015; revised 21 Jun 2015; accepted 26 Jul 2015; published 13 Aug 2015

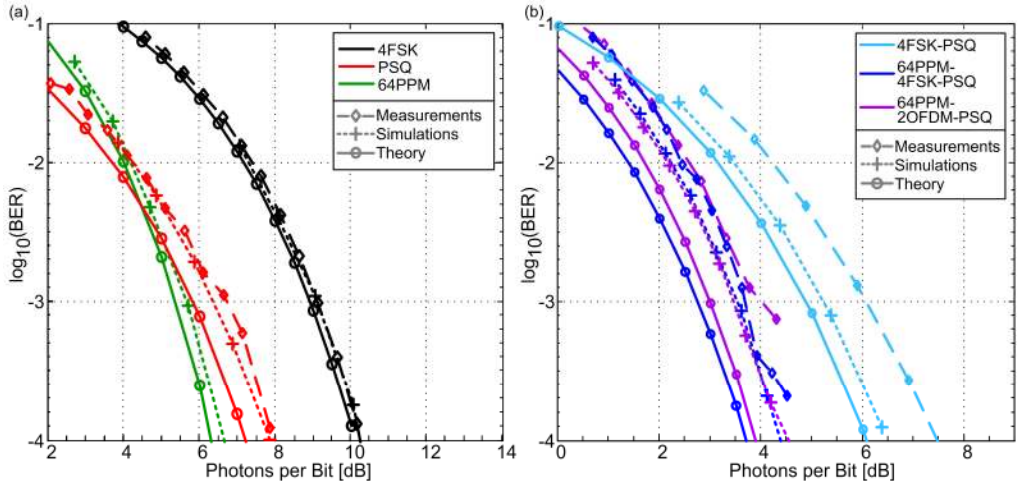

Fig. 5 Bit error ratio (BER) as a function of the number of photons per bit for different modulation formats. PSQ abbreviates the format PS-QPSK. (a) Individual modulation formats 4FSK, PS-PQSK, and 64PPM with sensitivities per bit of 9 dB, 7 dB, and 5 dB, respectively, at a target $\mathrm{BER} = 10^{-3}$. (b) Stacked modulation formats 4FSK-PS-QPSK, 64PPM-4FSK-PS-QPSK, and 64PPM-2OFDM-PS-QPSK. The limiting number of photons per bit reduces when stacking more modulation formats. The stacked format 64PPM-4FSK-PS-QPSK shows a limiting photon number per bit of 3.7 dB, slightly better than 64PPM-2OFDM-PSQ. Theoretically calculated BER for various modulation format stacks comprising 64PPM, 4FSK, PS-QPSK and including 2OFDM are shown for comparison.

Simulations and measurements differ slightly, but lie within the expected uncertainties with numerical simulations.

Figure 5(b) shows the BER for a number of modulation stacks, all measured at symbol rates of $R_{\mathrm{sym}} = (1/64) \times R_{\mathrm{slot}} = (1/64) \times 750\,\mathrm{MHz} \approx 11.7\,\mathrm{MHz}$. We start with 4FSK-PS-QPSK having 5 bit per symbol. In our measurements, we determine a limiting number of 6 dB photons per bit for a BER of 10^{-3}. It can be seen that the limiting number of photons per bit for 4FSK-PS-QPSK is by 1 dB better than for PS-QPSK. The simulations predict 5 dB photons per bit. The discrepancy stems from electronic hardware's bandwidth limitations, which could not be determined with sufficient accuracy and was left out for the simulations.

The next result shown in Fig. 5(b) refers to a 64PPM-4FSK-PS-QPSK stack with 11 bits per symbol. We achieved a record-low number of 2.3 PPB (3.7 dB) at a BER of 10^{-3}. Thus, stacking 4FSK-PS-QPSK with 64PPM results in an improvement of more than 2 dB compared to 4FSK-PS-QPSK.

Finally, we compare the 64PPM-4FSK-PS-QPSK stack with the frequency-division multiplexed 64PPM-2OFDM-PS-QPSK scheme. In this case, the 4FSK coding is replaced by a coding onto 2 OFDM subcarriers. This multiplexing technique leads to 12 bit per symbol instead of only 11 bit per symbol for the 4FSK case. Again, a sensitivity of about 2.4 PPB is found at a BER of 10^{-3}.

The analytical results discussed in the previous section compare well with measurement and simulations. We find for both PPM-FSK-PS-QPSK and 64PPM-2OFDM-PS-QPSK a small penalty of about 1 dB at $\mathrm{BER} = 10^{-3}$ against the analytical predictions. This penalty is most likely due to a non-ideal representation of continuous sine and cosine waves by the time-discrete and quantized outputs of our AWG. Additional impairments come through phase distortions due to the low-pass characteristic of the electrical devices, and through a non-ideal phase-estimation in the receiver.

The finding that the modulation stack 64PPM-4FSK-PS-QPSK and the modulation/multiplexing scheme 64PPM-2OFDM-PS-QPSK behave very similar, has already been explained above with the help of Fig. 3(b). Thus we will not discuss it here again.

#238307 Received 17 Apr 2015; revised 21 Jun 2015; accepted 26 Jul 2015; published 13 Aug 2015

Finally, we should comment on the effect of using the same laser as a sender in the transmitter and as a local oscillator at the receiver. Under the assumption that the QPSK symbol duration (i. e., the PPM time slot) is short, an independent high-quality local oscillator would not significantly influence the systems performance, and no penalty could be measured. This is true for our local oscillator laser with a 1 kHz linewidth where a phase drift from one symbol to the next is very small. In future, such a system would probably be operated at larger symbol rates such that drifts from one symbol to the next would even be smaller.

6. Conclusion

In this paper, we demonstrate stacking of PPM with FSK and PS-QPSK. We demonstrated experimentally a record-high receiver sensitivity of 2.3 photons per bit (3.7 dB) at $\mathrm{BER} = 10^{-3}$ by using 64PPM in combination with 4FSK and PS-QPSK. In stacking these modulation formats we were able to encode 11 bit in one 64PPM-4FSK-PSQPSK symbol. It was further shown that a similar sensitivity is obtained when encoding 12 bit in a 64 PPM-2OFDM-PS-QPSK symbol. Theoretical analysis and numerical simulations verified the experimental results. Stacking modulation formats is highly attractive for applications where best receiver sensitivity is required and spectral efficiency is of lesser importance, such as in free-space communication systems.

Appendix A: Measurement of the number of photons per bit

To determine the number of photons per bit that are required for reception with a target BER of 10^{-3}, two different measurement techniques are used.

First, the numbers of photons per bit are calculated from the average received signal power P_{Sig} as measured with a power meter.

With the center frequency f_c, Planck's constant h, the 64PPM symbol rate $R_{\mathrm{sym}} = (1/64) \times R_{\mathrm{slot}} = (1/64) \times 750\,\mathrm{MHz} \approx 11.7\,\mathrm{MHz}$ and the number of bits $n_{\mathrm{bit/sym}}$ per symbol, we find the number $N_{P\,\mathrm{bit}}$ of photons per bit as

$$N_{P\,\mathrm{bit}} = \frac{P_{\mathrm{Sig}}}{h f_c R_{\mathrm{bit}}} = \frac{P_{\mathrm{Sig}}}{h f_c R_{\mathrm{sym}} n_{\mathrm{bits/sym}}} \tag{3}$$

Here, for a 64PPM-4FSK-PSQPSK symbol $n_{\mathrm{bits/sym}} = 11$.

The second way to determine the number of photons per bit is by measuring the OSNR. In this experiment, the OSNR is measured with the help of a high-resolution optical spectrum analyzer with 20 MHz resolution to verify the results shown previously that are derived from the power meter. It is the same device from which the spectrum shown in Fig. 4(c) is derived. The $\mathrm{SNR_{bit}}$ can directly be derived from an OSNR measurement [17] and equals the number of photons per bit [23],

$$\mathrm{SNR_{bit}} = \frac{2B_{\mathrm{O}}}{R_{\mathrm{sym}} n_{\mathrm{bits/sym}}} \mathrm{OSNR} \tag{4}$$

According to the spectrum Fig. 2(c), the optical signal bandwidth is $B_{\mathrm{O}} = 6R_{\mathrm{slot}} = 6 \times 750\,\mathrm{MHz} = 4.5\,\mathrm{GHz}$. Note that for our definition of the OSNR the noise power is not measured in a 0.1 nm wide reference bandwidth, but rather measured in the actual signal bandwidth B_{O}. Therefore our values for OSNR describe the signal to noise power ratios of 4.5 GHz bandwidth.

The measured OSNR values are in good agreement with the photons per bit derived by the received signal power as shown in Fig. 6.

#238307 Received 17 Apr 2015; revised 21 Jun 2015; accepted 26 Jul 2015; published 13 Aug 2015

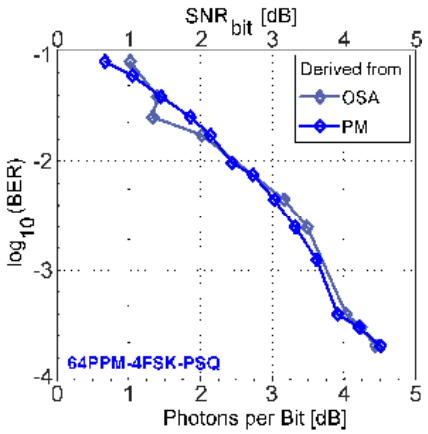

Fig. 6 Comparison of the results derived from the power meter (PM) and the optical spectrum analyzer (OSA) for 64PPM-4FSK-PS-QPSK.

Appendix B: Sensitivity of PPM, FSK and PS-QPSK formats

We assume a polarization-diversity receiver with an optical pre-amplifier, and we concentrate on coherent reception. We describe the received baseband signal in *x* and *y*-polarizations by the vector $\boldsymbol{\rho}(t) = r_x(t)\vec{\mathrm{e}}_x + r_y(t)\vec{\mathrm{e}}_y$ (orthogonal unit vectors $\vec{\mathrm{e}}_{x,y}$), which comprises the signal vector $\mathbf{s}(t)$ and the noise vector $\mathbf{n}(t)$,

$$\boldsymbol{\rho}(t) = \mathbf{s}(t) + \mathbf{n}(t), \quad \mathbf{s} = \begin{pmatrix} s_x \\ s_y \end{pmatrix} = \begin{pmatrix} I_x + \mathrm{j}Q_x \\ I_y + \mathrm{j}Q_y \end{pmatrix}, \quad \mathbf{n} = \begin{pmatrix} n_x \\ n_y \end{pmatrix} = \begin{pmatrix} n_{I,x} + \mathrm{j}n_{Q,x} \\ n_{I,y} + \mathrm{j}n_{Q,y} \end{pmatrix} \tag{5}$$

The noise terms of in-phase and quadrature in both polarizations are $n_{I,x,y}$ and $n_{Q,x,y}$, respectively. These noise terms are assumed to be independently Gaussian distributed with zero mean and variance $\sigma_{x,y}^2 = \sigma_{I,x,y}^2 = \sigma_{Q,x,y}^2 = \sigma^2$, since the amplified spontaneous emission (ASE) due to our pre-amplifying EDFAs is the dominant source of noise [17].

In the following, the bit error ratios of the constituents of the stacked modulation formats are considered separately, i.e., PPM, FSK, and PS-QPSK. Alternatively, the primary PPM format can also be followed by an OFDM step which replaces FSK. Because our PPM demodulation is different for FSK and OFDM coding, we have to adapt the calculated bit-error ratios accordingly.

PPM: PPM symbols are orthogonal, and the field in each time slot can be interpreted as an ASK signal: The received signal in each slot represents one ASK symbol having either the amplitude *A*, if there is a pulse, or the amplitude zero if the slot is empty. We therefore refer to the results from a sensitivity analysis for ASK signals [24] and adapt them for PPM.

In the present experiments, each PPM symbol is simultaneously sent with equal power in *x* and *y*-polarization. Our demodulation technique adds the amplitudes received in the *x*- and *y*-polarizations. We define a new amplitude quantity r_{FSK} for each time slot

$$r_{\mathrm{FSK}} = |r_x| + |r_y|, \quad r_{x,y} = s_{x,y} + n_{x,y} = I_{x,y} + n_{I,x,y} + \mathrm{j}\left(Q_{x,y} + n_{Q,x,y}\right). \tag{6}$$

This received amplitude quantity, which is impaired by noise, must be compared to the pure signal A_{FSK} of the amplitude in *x* and *y*-polarization

$$|s_x| = |s_y| \equiv A_{\mathrm{FSK}}, \text{ where } A_{\mathrm{FSK}}^2 \in \{0,\, \mathcal{E}_{\mathrm{slot}}/T_{\mathrm{slot}}\}. \tag{7}$$

As already mentioned, both polarizations carry the same power. The sum of these powers $\frac{1}{2}|s|_x^2 + \frac{1}{2}|s|_y^2 = A_{\mathrm{FSK}}^2$ in an occupied PPM slot represents the energy $\mathcal{E}_{\mathrm{slot}}$ per slot duration T_{slot},

#238307 Received 17 Apr 2015; revised 21 Jun 2015; accepted 26 Jul 2015; published 13 Aug 2015

and is zero elsewhere. The probability density function (PDF) p_r of each of the two absolute-value terms $r = |r_{x,y}|$ in Eq. (4) is given by the Rice PDF in an occupied slot with $A = A_{\mathrm{FSK}} \neq 0$, and by the Rayleigh PDF for an empty slot with $A = A_{\mathrm{FSK}} = 0$, respectively [25] (p. 48, Eq. (2).3-43), (2.3-56))

$$p_r(r, A) = \begin{cases} \dfrac{r}{\sigma^2} \mathrm{e}^{-\frac{r^2+A^2}{2\sigma^2}} I_0\left(\dfrac{Ar}{\sigma^2}\right) & \text{for} \quad r > 0 \\ 0 & \text{for} \quad r \le 0. \end{cases} \tag{8}$$

The random variables $|r_x|$ and $|r_y|$ are statistically independent with respect to their noise contributions n_x and n_y, therefore their sum $r_{\mathrm{FSK}} = |r_x| + |r_y|$ results in a PDF which is a convolution [24]

$$p_{\mathrm{FSK}}(r_{\mathrm{FSK}}, A_{\mathrm{FSK}}) = p_r(|r_x|, A_{\mathrm{FSK}}) * p_r(|r_y|, A_{\mathrm{FSK}}) = (p_r * p_r)(r_{\mathrm{FSK}}, A_{\mathrm{FSK}}) \tag{9}$$

We evaluate this convolution numerically.

In the case of 64PPM-2OFDM we transmit per occupied PPM-slot two OFDM subcarriers, which are subscripted with α and β. We apply an FFT to the signal in each PPM time slot and for each polarization, and look at the 2 × 2 complex Fourier coefficients $s_{x,y,\alpha}$ and $s_{x,y,\beta}$ which are associated with the two OFDM subcarrier signals,

$$s_\alpha = \begin{bmatrix} s_{x\alpha} \\ s_{y\alpha} \end{bmatrix} = \begin{bmatrix} I_{x\alpha} + \mathrm{j}Q_{x\alpha} \\ I_{y\alpha} + \mathrm{j}Q_{y\alpha} \end{bmatrix} \quad , \quad s_\beta = \begin{bmatrix} s_{x\beta} \\ s_{y\beta} \end{bmatrix} = \begin{bmatrix} I_{x\beta} + \mathrm{j}Q_{x\beta} \\ I_{y\beta} + \mathrm{j}Q_{y\beta} \end{bmatrix} \tag{10}$$

We proceed as in Eq. (4) and form the sum of the moduli for x and y-polarizations $r_{\mathrm{FSK}\alpha} = |r_{x\alpha}| + |r_{y\alpha}|$ and $r_{\mathrm{FSK}\beta} = |r_{x\beta}| + |r_{y\beta}|$ for each subcarrier α and β,

$$\begin{aligned} r_{\mathrm{OFDM}} &= r_{\mathrm{FSK}\alpha} + r_{\mathrm{FSK}\beta} = |r_{x\alpha}| + |r_{y\alpha}| + |r_{x\beta}| + |r_{y\beta}| \\ &= \left|I_{x\alpha} + n_{I,x\alpha} + \mathrm{j}\left(Q_{x\alpha} + n_{Q,x\alpha}\right)\right| + \left|I_{y\alpha} + n_{I,y\alpha} + \mathrm{j}\left(Q_{y\alpha} + n_{Q,y\alpha}\right)\right| \\ &\quad + \left|I_{x\beta} + n_{I,x\beta} + \mathrm{j}\left(Q_{x\beta} + n_{Q,x\beta}\right)\right| + \left|I_{y\beta} + n_{I,y\beta} + \mathrm{j}\left(Q_{y\beta} + n_{Q,y\beta}\right)\right| \end{aligned} \tag{11}$$

with

$$|s_{x\alpha}| = |s_{x\beta}| = |s_{y\alpha}| = |s_{y\beta}| \equiv A_{\mathrm{OFDM}} \quad \text{and} \quad 2A_{\mathrm{OFDM}}^2 \in \{0, \mathcal{E}_{\mathrm{slot}}/T_{\mathrm{slot}}\} \tag{12}$$

Again, the sum of the pure signal powers $\frac{1}{2}|s_{x\alpha}|^2 + \frac{1}{2}|s_{x\alpha}|^2 + \frac{1}{2}|s_{y\alpha}|^2 + \frac{1}{2}|s_{y\beta}|^2 = 2A_{\mathrm{OFDM}}^2$ in an occupied PPM slot represents the energy $\mathcal{E}_{\mathrm{slot}}$ per slot duration T_{slot}, and is zero elsewhere. The random variables $|r_{x\alpha}|$, $|r_{y\alpha}|$, $|r_{x\beta}|$ and $|r_{y\beta}|$ are statistically independent with respect to their noise contributions, therefore the PDF of r_{OFDM} is computed by the convolution

$$\begin{aligned} p_{\mathrm{OFDM}}(r_{\mathrm{OFDM}}, A_{\mathrm{OFDM}}) &= p_{\mathrm{FSK}}(r_{\mathrm{FSK}\alpha}, A_{\mathrm{OFDM}}) * p_{\mathrm{FSK}}(r_{\mathrm{FSK}\beta}, A_{\mathrm{OFDM}}) \\ &= (p_{\mathrm{FSK}} * p_{\mathrm{FSK}})(r_{\mathrm{OFDM}}, A_{\mathrm{OFDM}}) \end{aligned} . \tag{13}$$

Again we evaluate this convolution numerically.

Now that we know the PDFs of the quantities r_{FSK} and r_{OFDM} which we want to detect, the resulting bit error ratio (BER, bit error probability) can be calculated. The PPM symbol error ratio (SER, symbol error probability) can be expressed according to [6] (Eq. (4).34)) in terms of the probability P_{c} to detect a correct symbol,

$$\mathrm{SER}_{\mathrm{PPM}} = 1 - P_{\mathrm{c}} \ . \tag{14}$$

#238307 Received 17 Apr 2015; revised 21 Jun 2015; accepted 26 Jul 2015; published 13 Aug 2015

Since *M*-ary PPM is an orthogonal signaling scheme with equal energy in each symbol, an optimum detector choses the signal with the largest cross-correlation between received symbol and any of the *M* possible symbols, i. e., the slot with the maximum value $r_1 = \max(r_{\mathrm{FSK}})$ or $r_1 = \max(r_{\mathrm{OFDM}})$ within a PPM symbol is regarded to carry the information. Mathematically it is advantageous to calculate first the probability of a correct decision. The probability to correctly detect the information in slot 1 is the joint probability of the $M-1$ independent events that the unoccupied slots have amplitudes smaller than r_1, averaged with the PDF that actually r_1 occurs,

$$P_{\mathrm{c}} = \int_{-\infty}^{\infty} \left[\int_{-\infty}^{r_1} p_0(r_0)\,\mathrm{d}r_0 \right]^{M-1} p_1(r_1)\,\mathrm{d}r_1 = \int_{-\infty}^{\infty} \left[1 - \int_{r_1}^{\infty} p_0(r_0)\,\mathrm{d}r_0 \right]^{M-1} p_1(r_1)\,\mathrm{d}r_1 \,. \qquad (15)$$

Depending on the use of FSK or OFDM, the function $p_0(r_0)$ is the probability density function of the signal in an empty PPM slot, namely $p_{\mathrm{FSK}}(r_0, A_{\mathrm{FSK}})$ or $p_{\mathrm{OFDM}}(r_0, A_{\mathrm{OFDM}})$ for $A_{\mathrm{FSK}} = 0$ or $A_{\mathrm{OFDM}} = 0$, respectively. For occupied slots the PDF $p_1(r_1)$ equals $p_{\mathrm{FSK}}(r_1, A_{\mathrm{FSK}})$ or $p_{\mathrm{OFDM}}(r_1, A_{\mathrm{OFDM}})$ for $A_{\mathrm{FSK}} = \sqrt{\mathcal{E}_{\mathrm{slot}}/T_{\mathrm{slot}}}$ or $A_{\mathrm{OFDM}} = \sqrt{\mathcal{E}_{\mathrm{slot}}/(2T_{\mathrm{slot}})}$, respectively. The PDFs $p_{\mathrm{FSK,OFDM}}$ were specified in Eq. (9) and Eq. (13).

Ultimately, we are interested in the BER rather than the SER. The BER is obtained as follows: For a correct symbol any of the *M* possible slots is occupied with equal probability. The alphabet consists of *M* symbols. Therefore an erroneous symbol is left to occupy any of $M-1$ possible time slots. Because the symbol error probability in Eq. (14-15) relates to all possible statistically independent slots in a PPM symbol, the error probability $\mathrm{SER}_{\mathrm{PPM}}/(M-1)$ for a specific symbol at a given slot position is smaller than .. by a factor of $1/(M-1)$.

The set of *M* symbols transports a number of $k = \log_2(M)$ bits. To find the probability $\mathrm{BER}_{\mathrm{PPM}}$ for a bit error one needs to determine how many of the *k* bits will be corrupted if one symbol is erroneous. Assuming that any one of the bits in a specific symbol is wrong with equal probability, there are half the number of symbols $M/2 = 2^{k-1}$ which share this bit and are therefore wrong with equal probability. Thus the bit error ratio increases over the symbol error ratio for a specific symbol by a factor of 2^{k-1}. As a consequence, the probability for detecting a wrong bit in a specific symbol is [21] (Eq. (4.4-12))

$$\mathrm{BER}_{\mathrm{PPM}} = \frac{2^{k-1}}{2^k - 1}\mathrm{SER}_{\mathrm{PPM}} = \frac{M}{2}\frac{1}{M-1}\mathrm{SER}_{\mathrm{PPM}} \qquad (16)$$

If the BER as a function of photons per bit is of interest, we need to specify the receiver more closely. Our pre-amplified receiver has a power gain G, an inversion factor n_{sp} and an electrical bandwidth B. Substituting the PDFs in Eq. (15) by Eq. (9) or Eq. (13), the BER for PPM can be calculated, Eq. (16). It depends on the signal energy $\mathcal{E}_{\mathrm{slot}}$ per slot (which is equivalent to the total signal energy $\mathcal{E}_s$ for a symbol because only one slot can be occupied), and on the noise spectral density of amplified spontaneous emission $N_{\mathrm{ASE}} = n_{\mathrm{sp}}(G-1)hf_{\mathrm{c}}$ per polarization [6,17,21], where n_{sp} is the inversion factor and hf_{c} represents the photon energy. The energy of a symbol in both polarizations is $\mathcal{E}_s = GN_{P\mathrm{sym}}hf_{\mathrm{c}}$ if $N_{P\mathrm{sym}}$ denotes the number of photons per symbol. The signal-to-noise power ratio per polarization is

$$\mathrm{SNR}_x = \frac{\frac{1}{2}A_{\mathrm{FSK}}^2}{\sigma_x^2} = \frac{\frac{1}{2}\mathcal{E}_s}{N_{\mathrm{ASE}}} = \frac{\frac{1}{2}GN_{P\mathrm{sym}}hf_{\mathrm{c}}}{n_{\mathrm{sp}}(G-1)hf_{\mathrm{c}}} \approx \frac{1}{2}N_{P\mathrm{sym}}, \quad N_{P\mathrm{bit}} = \frac{N_{P\mathrm{sym}}}{n_{\mathrm{bit/sym}}}. \qquad (17)$$

The approximation holds for a fully inverted amplifier $n_{\mathrm{sp}} \approx 1$ and a large power gain $G \gg 1$ [6]. The number of photons per bit results from the number of photons per symbol divided by the number of bits $n_{\mathrm{bits/sym}}$ encoded in one symbol. The resulting $\mathrm{BER}_{\mathrm{PPM}}$ for pure 64PPM according to Eq. (14)-(15) and (9), i. e., without subsequent OFDM multiplexing, is depicted in Fig. 3.

FSK: The condition that the *N*-ary FSK frequency spacing equals the reciprocal symbol rate establishes orthogonal signaling, and in this respect FSK as employed in our experiments

#238307 Received 17 Apr 2015; revised 21 Jun 2015; accepted 26 Jul 2015; published 13 Aug 2015

is closely related to PPM [21]. For 4FSK we use four orthogonal frequencies having a frequency spacing of $nR_{\mathrm{slot}} = n\Delta f$ with $n \in \{\pm 1, \pm 2\}$ and find the analytical notation:

$$s_n(t) = A\cos(2\pi n \times \Delta f t) + \mathrm{j}\ A\sin(2\pi n \times \Delta f t) = A\exp(\mathrm{j}\ 2\pi n \times \Delta f t) \qquad (18)$$

Thus our FSK alphabet realizes an orthogonal signaling scheme having correlation coefficients of 1 or 0 [21,26]. In this sense our 4FSK signaling resembles 4PPM.

However, in our experiment we use a demodulation technique in the frequency domain. We do so by applying a Fourier transform to the complex FSK symbols during a PPM time slot, and determine the signal sent by the maximum modulus of the Fourier transform. Thus, in analogy to Eq. (5) the received signal in the frequency domain reads

$$\begin{aligned}
\breve{\boldsymbol{\rho}}(f) &= \int_{-\infty}^{+\infty} [\mathbf{s}(t) + \mathbf{n}(t)]\, \mathrm{e}^{-\mathrm{j}2\pi f t}\, \mathrm{d}t, \\
\breve{r}_x(f) &= \int_{-\infty}^{+\infty} \left[I_x(t) + n_{I,x}(t) + \mathrm{j}\left(Q_x(t) + n_{Q,x}(t)\right)\right] \mathrm{e}^{-\mathrm{j}2\pi f t}\, \mathrm{d}t, \\
\breve{r}_y(f) &= \int_{-\infty}^{+\infty} \left[I_y(t) + n_{I,y}(t) + \mathrm{j}\left(Q_y(t) + n_{Q,y}(t)\right)\right] \mathrm{e}^{-\mathrm{j}2\pi f t}\, \mathrm{d}t.
\end{aligned} \qquad (19)$$

Only the four discrete frequencies f_n with $n \in \{\pm 1, \pm 2\}$ of the FFT are of interest for our signal demodulation. For extracting the FSK information, we define

$$\breve{r}_{\mathrm{F}}(f_n) = \left|\breve{r}_x(f_n)\right| + \left|\breve{r}_y(f_n)\right|, \qquad \breve{r}_{x,y}(f_n) = \int_{f_n - \frac{1}{2}\Delta f}^{f_n + \frac{1}{2}\Delta f} \breve{r}_{x,y}(f)\, \mathrm{d}f\,. \qquad (20)$$

We then find the maximum value of $\breve{r}_{\mathrm{F}}(f_n)$ for $n \in \{\pm 1, \pm 2\}$. Thus, for the demodulation of the FSK information we apply a similar demodulation scheme as in PPM and therefore expect a similar receiver sensitivity. Thus for *N*-ary FSK, Eq. (9) and Eq. (14)-(17) hold when substituting $M = N$. The result is depicted for 4FSK in Fig. 3.

PS-QPSK: This modulation format comprises a set of bi-orthogonal signals with 8 constellation points and complementary bit encoding (see [26] pp. 198-203). As suggested in [10], for comparison see also [21], Eq. (4).4-25, p. 208, we use the inverted bit pattern for anti-correlated symbols for bit encoding to achieve a minimum BER for a given SER. As a result, we find the BER [10]:

$$\mathrm{BER}_{\mathrm{PSQ}} = \frac{1}{2\sqrt{\pi}} \int_{-\infty}^{+\infty} \left(3 - 3\,\mathrm{erfc}(r) + \mathrm{erfc}^2(r)\right) \mathrm{erfc}(r) \exp\left[-\left(r - \sqrt{\frac{\mathcal{E}_{\mathrm{s}}}{N_0}} \right)^2 \right] \mathrm{d}r \qquad (21)$$

The quotient $N_{P\mathrm{sym}} = \mathcal{E}_{\mathrm{s}} / N_0$ describes the symbol energy divided by the noise spectral density and equals the number of photons per symbol. The result of this equation is depicted in Fig. 3.

Acknowledgments

We acknowledge support from Keysight Technologies (formerly Agilent Technologies' Electronic Measurement Group), NKT Photonics, the Institute of Radio-Frequency and Electronics at Karlsruhe Institute of Technology (KIT), and the Institute of Robust Power Semiconductor Systems of the University of Stuttgart. We further acknowledge support by the Open Access Publishing Fund of KIT.